Letter

Vol. 45, No. 19 / 1 October 2020 / Optics Letters 5381

Optics Letters

# Photonic scanning receiver for wide-range microwave frequency measurement by photonic frequency octupling and in-phase and quadrature mixing

JINGZHAN SHI,[1,2] FANGZHENG ZHANG,[1,*] YUEWEN ZHOU,[1] SHILONG PAN,[1] YIPING WANG,[2] AND DE BEN[1]

[1]Key Laboratory of Radar Imaging and Microwave Photonics, Ministry of Education, Nanjing University of Aeronautics and Astronautics, Nanjing 210016, China

[2]Jiangsu Key Lab on Opto-Electronic Technology, School of Physical Science and Technology, Nanjing Normal University, Nanjing 210046, China

*Corresponding author: zhangfangzheng@nuaa.edu.cn

Received 22 June 2020; revised 27 July 2020; accepted 3 August 2020; posted 5 August 2020 (Doc. ID 400918); published 21 September 2020

**A photonic scanning receiver with optical frequency scanning and electrical intermediate frequency envelope detection is proposed to implement wide-range microwave frequency measurement. This system applies photonic in-phase and quadrature frequency mixing to distinguish and measure the signals in two frequency bands that mirror each other. Combined with the photonic frequency octupling technique, the proposed system has a frequency measurement range that is 16 times that of the sweeping range of the electrical signal source. Besides, optical frequency sweeping with up and down chirps is used to relax the requirement for precise synchronization between the sweeping source and the analog-to-digital converter. In the experiment, using an electrical sweeping local oscillator having a bandwidth of 1.75 GHz, the system achieves a frequency measurement range as large as 28 GHz. The measurement errors are kept within 24 MHz with an average error of 9.31 MHz.** 

https://doi.org/10.1364/OL.400918

Microwave frequency measurement has wide applications in communication and electronic warfare applications [1,2]. Photonic technologies have been proposed to implement microwave frequency measurement with considerably enlarged frequency measurement range [3–9]. Recently, we have proposed a photonic scanning receiver-based microwave frequency measurement system [10–12], which is achieved using optical-domain frequency scanning and electrical-domain intermediate frequency (IF) envelope detection. This method makes the most of current electrical signal generators with high precision and flexibility and greatly expands the operation frequency by microwave photonic frequency multiplication and mixing. However, a potential problem with this method is that it cannot distinguish a signal with its image frequency. Therefore, an image-rejection filter is equipped in the receiver to select one of the two bands that mirror each other. Rough elimination of the image frequency band with the filter reduces the measurement range in the meantime. In this method, the frequency to be measured is mapped to the time position of a short pulse. Thus, precise synchronization between the sweeping source and the analog-to-digital converter (ADC) is required to achieve accurate frequency measurement. In this Letter, we propose an improved photonic scanning receiver to solve the previous problems. First, microwave photonic in-phase and quadrature (I/Q) mixing is applied to avoid the measurement ambiguity between the two frequency bands that mirror each other, which makes it feasible to simultaneously measure the signals in these two frequency bands. Second, optical frequency sweeping with up and down chirps is utilized, instead of the up-chirp frequency sweeping in the previous work. This relaxes the requirements for synchronization between the frequency sweeping source and the ADC. Furthermore, a photonics-based frequency octupling technique is used to enlarge the frequency sweeping range.

Figure 1 shows the schematic diagram of the improved photonic scanning receiver. The electrical local oscillator (LO) generates a linearly frequency modulated (LFM) signal with up and down chirps, of which the instantaneous frequency is expressed as

$$f_{\mathrm{L}}(t)=\begin{cases} f_0+kt, & 0\le t\le \frac{T_{\mathrm{L}}}{2} \\ f_0+k\frac{T_{\mathrm{L}}}{2}-k\left(t-\frac{T_{\mathrm{L}}}{2}\right), & \frac{T_{\mathrm{L}}}{2}<t\le T_{\mathrm{L}} \end{cases}, \tag{1}$$

where $f_0$ and $T_{\mathrm{L}}$ are the initial frequency and the temporal period of the LO signal. The chirp rate is $k$ in the time from zero to $T_{\mathrm{L}}/2$, while the chirp rate is $-k$ in the time from $T_{\mathrm{L}}/2$ to $T_{\mathrm{L}}$. The bandwidth of this signal is $kT_{\mathrm{L}}/2$. The LO signal is split into two signals through a microwave 90° hybrid. The obtained two signals with a 90° phase difference are used to drive a dual-parallel Mach–Zehnder modulator (DPMZM) to modulate a continuous-wave (CW) light that is generated by a laser diode (LD). In the DPMZM, the two sub-MZMs are biased at the maximum transmission point (MATP) to suppress the odd-order modulation sidebands, and the main MZM (MZMc) is also biased at the MATP. This way, the obtained optical signals mainly contains the optical carrier and the ±fourth-order modulation sidebands [13]. Then, a dual-output optical band-pass filter (DOBPF) is used to select and separate the ±fourth-order sidebands into two channels. In the upper channel, the −fourth-order sideband is modulated by the signal under test (SUT) at an MZM, which is biased at the minimum transmission point (MITP). After the MZM, ±first-order modulation sidebands at frequencies of $f_c - 4f_L \pm f_x$ are generated, in which $f_c$ is the frequency of the laser source and $f_x$ is the frequency of the SUT. After the MZM, an erbium-doped fiber amplifier (EDFA) is used to boost the optical power and an OBPF is followed to select the modulation sideband at the frequency of $f_c - 4f_{\mathrm{L}} + f_{\mathrm{x}}$. To get the I/Q mixing signals, the modulation sideband at frequency of $f_c - 4f_{\mathrm{L}} + f_{\mathrm{x}}$ is then coupled with the +fourth-order sideband at frequency of $f_c + 4f_{\mathrm{L}}$ from the lower channel of the DOBPF through an optical 90° hybrid followed by two balanced photodetectors (BPDs) [14], as written by

$$\begin{bmatrix} v_{\mathrm{I}}(t) \\ v_{\mathrm{Q}}(t) \end{bmatrix} \propto \begin{bmatrix} 1 & 1 \\ j & -j \end{bmatrix} \begin{bmatrix} e^{j2\pi(8f_{\mathrm{L}}-f_{\mathrm{x}})t} \\ e^{j2\pi(f_{\mathrm{x}}-8f_{\mathrm{L}})t} \end{bmatrix}. \tag{2}$$

The spectra of the I/Q mixing signals are

$$\begin{bmatrix} S_{\mathrm{I}}(f) \\ S_{\mathrm{Q}}(f) \end{bmatrix} = \begin{bmatrix} 1 & 1 \\ j & -j \end{bmatrix} \begin{bmatrix} \delta\,[f-(8f_{\mathrm{L}}-f_{\mathrm{x}})] \\ \delta\,[f-(f_{\mathrm{x}}-8f_{\mathrm{L}})] \end{bmatrix}, \tag{3}$$

where $\delta(f)$ is the impulse function.

Following the two BPDs, the I/Q mixing signals pass through two narrow-band IF filters (IF filter1, 2) having the same center frequency of $f_{\mathrm{I}}(f_{\mathrm{I}} > 0)$, respectively. Assuming that the narrow-band IF filters have an ideal transmission function of $\delta(f - f_{\mathrm{I}})$, the spectra of the IF I/Q signals at the output ports of IF filter1 and IF filter2 are

$$\begin{bmatrix} S_{\mathrm{I1}}(f) \\ S_{\mathrm{Q1}}(f) \end{bmatrix} = \begin{bmatrix} S_{\mathrm{I}}(f) \\ S_{\mathrm{Q}}(f) \end{bmatrix} \delta(f-f_{\mathrm{I}})\,. \tag{4}$$

Then, the two IF signals are coupled at a 2 × 2 microwave 90° hybrid. The spectra of the obtained two signals after the 2 × 2 microwave 90° hybrid are

$$\begin{bmatrix} S_1(f) \\ S_2(f) \end{bmatrix} = \begin{bmatrix} j & 1 \\ 1 & j \end{bmatrix} \begin{bmatrix} S_{\mathrm{I1}}(f) \\ S_{\mathrm{Q1}}(f) \end{bmatrix}$$
$$= \begin{bmatrix} 2j\delta\,[f_{\mathrm{I}}-(8f_{\mathrm{L}}-f_{\mathrm{x}})]\,\delta(f-f_{\mathrm{I}}) \\ 2\delta\,[f_{\mathrm{I}}-(f_{\mathrm{x}}-8f_{\mathrm{L}})]\,\delta(f-f_{\mathrm{I}}) \end{bmatrix}. \tag{5}$$

Next, two envelope detectors (EDs) are used to detect the envelopes of the signals from the 2 × 2 microwave 90° hybrid. According to the spectra in Eq. (5), the obtained envelope signals are

$$e_1(t) \propto \delta\,[f_{\mathrm{I}}-(8f_{\mathrm{L}}-f_{\mathrm{x}})] = \begin{cases} \neq 0, & 8f_{\mathrm{L}}(t) = f_{\mathrm{x}} + f_{\mathrm{I}} \\ 0, & \text{else} \end{cases}$$
$$e_2(t) \propto \delta\,[f_{\mathrm{I}}-(f_{\mathrm{x}}-8f_{\mathrm{L}})] = \begin{cases} \neq 0, & 8f_{\mathrm{L}}(t) = f_{\mathrm{x}} - f_{\mathrm{I}} \\ 0, & \text{else} \end{cases}. \tag{6}$$

It can be seen from Eq. (6) that the frequency to be measured ($f_{\mathrm{x}}$) is related to the time positions of the pulses in the obtained envelope signals. For a single input frequency, there are two pulses in one period (at $t_1$ and $t_2$ in Fig. 1) because of the frequency sweeping with both up and down chirps. The frequency can be measured once the temporal interval between the two pulses is known through analyzing the digital signals sampled by an ADC. According to Eq. (1) and Eq. (6), the frequency to be measured can be acquired by

$$f_{\mathrm{x}} = \begin{cases} 8f_0 + 4k[T_{\mathrm{L}} - (t_2 - t_1)] - f_{\mathrm{I}}, \\ \text{if } \exists 0 \le t_1 \le t_2 \le T_{\mathrm{L}} \text{ satisfy "} e_1(t_1) \text{ and } e_1(t_2) \neq 0\text{"} \\ 8f_0 + 4k[T_{\mathrm{L}} - (t_2 - t_1)] + f_{\mathrm{I}}, \\ \text{if } \exists 0 \le t_1 \le t_2 \le T_{\mathrm{L}} \text{ satisfy "} e_2(t_1) \text{ and } e_2(t_2) \neq 0\text{"} \end{cases}. \tag{7}$$

In Eq. (7), the frequency is estimated through a relative time of $t_2 - t_1$, without the need to know the pulse position referenced to the start time of frequency sweeping. Compared with the previous work, this is an obvious improvement that can relax the requirement for precise synchronization between the electrical LO and the ADC.

Another important feature of the proposed system is that it can distinguish the signals in the frequency band of $8f_L - f_{\mathrm{I}}$ and its image frequency band of $8f_{\mathrm{L}} + f_{\mathrm{I}}$, which is derived by using photonic I/Q mixing. It should be noted that, although this function can be implemented employing two electric image-rejection mixers, the operation bandwidth and image-rejection ratio would lag behind the photonic implementation [14]. In each channel of our system, the frequency measurement range of $4kT_{\mathrm{L}}$ is eight times the frequency sweeping range of the electrical LO ($kT_{\mathrm{L}}/2$). If there is no overlapping between the two measurable frequency bands (requiring $f_{\mathrm{I}} > 2kT_{\mathrm{L}}$), the total frequency measurement range reaches $8kT_{\mathrm{L}}$, which is 16 times as large as the frequency sweeping range of the electrical

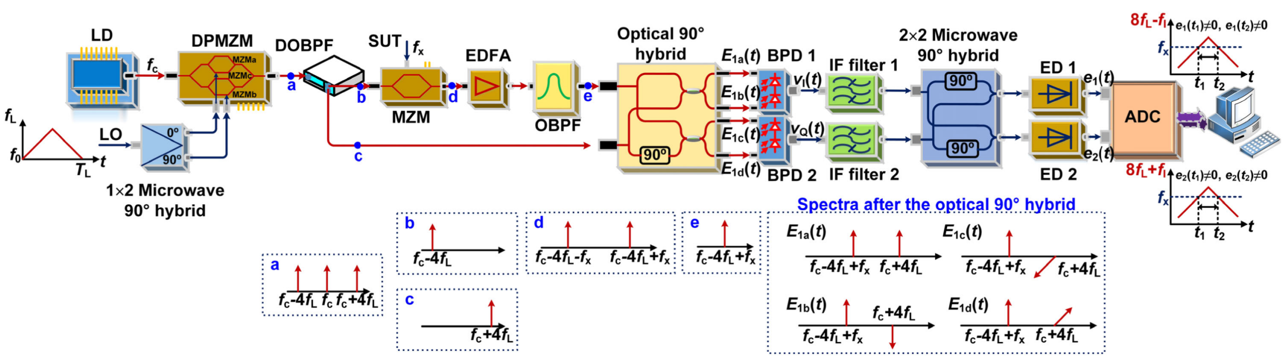


**Fig. 1.** Schematic diagram of the proposed photonic scanning receiver for wide-range microwave frequency measurement.

LO. Such a large frequency measurement range is attributed to the photonics-based frequency octupling operation.

An experiment is performed to verify the feasibility of the proposed system. In the experiment, the parameters $f_0$, $k$, and $T_L$ of the electrical LO signal are set to 2.75 GHz, 175 MHz/μs, and 20 μs, respectively, and the bandwidth of the LO signal is 1.75 GHz. Two band-pass filters having the same center frequency of 9.953 GHz and the same 3 dB bandwidth of 15 MHz are used as the IF filters. According to Eq. (7), the experimental system can measure the frequency in the range from 12.047 GHz to 26.047 GHz, and its image frequency in the range from 31.953 GHz to 45.953 GHz. The total frequency measurement range is 28 GHz. After passing through the microwave 90° hybrid (Narda, bandwidth 2–18 GHz), the two LO signals modulate a CW light emitted from the LD (wavelength: 1550.526 nm) at the DPMZM (Fujitsu FTM7962EP, 3 dB bandwidth: 22 GHz). By properly biasing the DPMZM, the desired optical carrier and the ±fourth-order modulation sidebands are generated in the spectrum, which is shown by the black-solid curve in Fig. 2(a). The response of the DOBPF (Finisar, Waveshaper 4000S) and the spectra at its two output ports (1# and 2#) are also shown in Fig. 2(a). It can be seen that the ±fourth-order modulation sidebands are successfully separated with the optical carrier suppressed by 42 dB. The −fourth-order modulation sideband is modulated by the SUT that is generated by a microwave signal generator (Keysight E8257D) at an MZM (Fujitsu FTM7938EZ, 3 dB bandwidth: 32 GHz) biased at the MITP. When the frequency of the SUT is set to 24 GHz, the optical spectrum after the MZM is shown in Fig. 2(b), in which the ±first-order modulation sidebands dominate in the spectrum. The optical signal after the MZM is amplified by an EDFA (Amonics AEDFA-35-B-FA). Then, the +first-order sideband is selected by the OBPF (Yenista XTM-50/S) having a response shown as the red-dashed curve in Fig. 2(b). The optical spectrum after the OBPF is shown by the blue-dotted curve in Fig. 2(b), where the desired +first-order sideband has a power of 52 dB higher than the residual −first-order sideband. The +fourth-order modulation sideband at

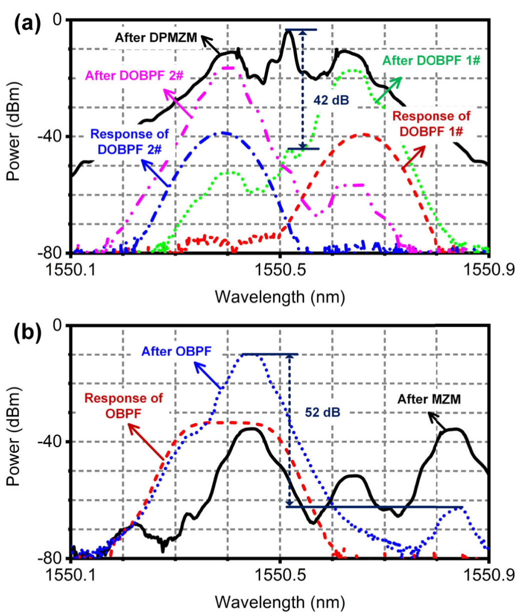


**Fig. 2.** Measured optical spectra of the signals (a) after the DPMZM and the DOBPF and (b) after the MZM and the OBPF.

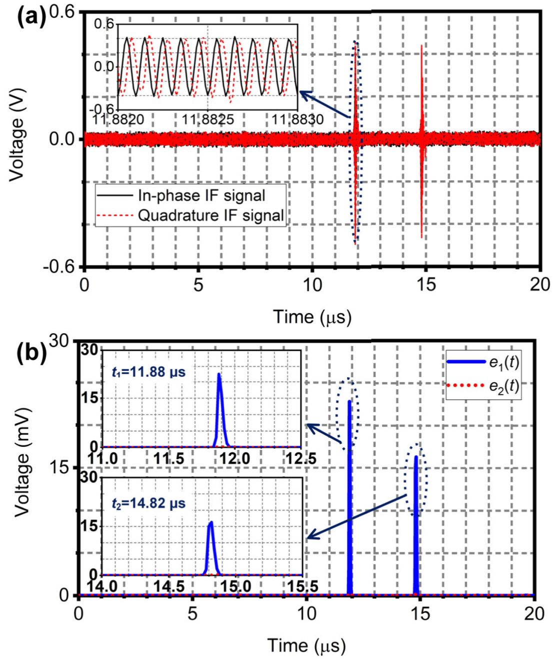


**Fig. 3.** Waveforms of (a) the signals at the output of the IF filters and (b) the envelope signals when the frequency under test is 24 GHz.

the output port of the DOBPF and the optical signal after the OBPF are sent to an optical 90° hybrid (Kylia COH28) followed by a pair of BPDs ($u^2t$ photonics BPDV2150R). The generated electrical signals are filtered by the IF filters to obtain the I/Q IF signals. When the frequency of the SUT is 24 GHz, the waveforms of the I/Q IF signals are acquired by a real-time oscilloscope with a sampling rate of 80 GSa/s (Keysight DSO-X 92504 A). The recorded waveforms in a period of 20 μs are plotted in Fig. 3(a). It can be seen from the zoom-in view of one of the pulses in Fig. 3(a) that the quadrature IF signal has a phase lag of 90° compared with the in-phase IF signal, indicating successful I/Q mixing is achieved. The envelopes of the signals after the 2 × 2 microwave 90° hybrid (Pulsar, bandwidth 0.5–10 GHz) are detected by two EDs (Agilent 8474C, bandwidth: 0.01–33 GHz), respectively. The two envelope signals are recorded by two channels of the oscilloscope, both of which have a sampling rate of 50 MSa/s. The waveforms of the two envelop signals, denoted by $e_1(t)$ and $e_2(t)$, are plotted in Fig. 3(b). As can be seen, two short pulses appear in signal $e_1(t)$, and no signal is detected in signal $e_2(t)$. The temporal positions of the two pulses in $e_1(t)$ are 11.88 μs and 14.82 μs, respectively, with an interval of 2.94 μs. Based on Eq. (7), the frequency of the SUT is measured to be 23.989 GHz. The measurement error is calculated to be 11 MHz.

To demonstrate that the proposed system can measure the signals in two image frequency bands, the frequency of the SUT is set to 43.906 GHz, which is the image frequency of the previous 24 GHz. In this case, the I/Q IF signals and the detected envelopes in one period are shown in Fig. 4(a) and Fig. 4(b), respectively. In Fig. 4(a), the phase of the quadrature IF signal is leading by 90° compared with that of the in-phase IF signal, which is different from the result in Fig. 3(a) when the SUT is 24 GHz. In Fig. 4(b), the two pulses only appear in the envelope signal $e_2(t)$, and their temporal positions are 16.24 μs and 19.16 μs, respectively. The time interval between the two

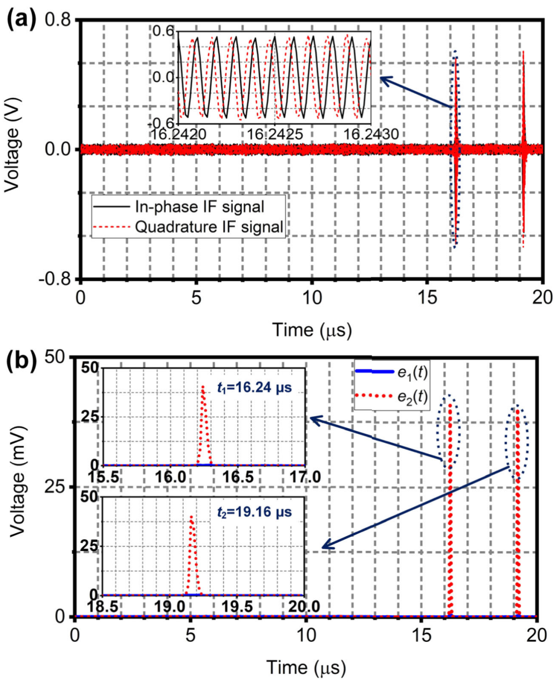


**Fig. 4.** Waveforms of (a) the signals at the output of the IF filters and (b) the envelope signals when the frequency under test is 43.906 GHz.

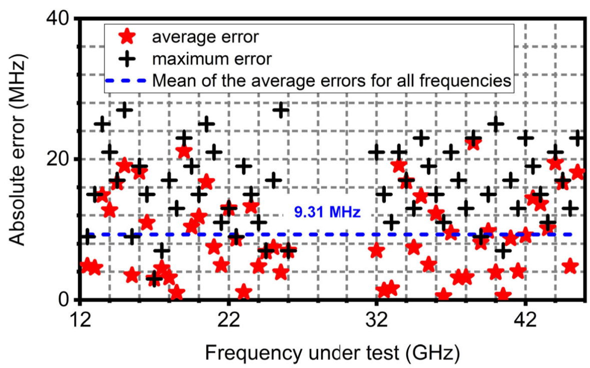


**Fig. 5.** Measurement errors versus frequencies in 28-GHz measurement range.

pulses is 2.92 μs, and the frequency of the SUT is measured to be 43.909 GHz with an absolute measurement error as low as 3 MHz.

Finally, to check the measurement accuracy within the whole frequency measurable range, the frequency of the SUT is tuned from 12.5 GHz to 26 GHz and then from 32 GHz to 45.5 GHz with a step of 0.5 GHz. For each frequency, 83-times repeated measurements are conducted, and the averaged measurement error as well as the maximum measurement error is calculated and shown in Fig. 5. As can be seen, the average measurement errors and the maximum measurement errors for all the frequencies are kept within 24 MHz and 28 MHz, respectively. The mean of the average errors considering all the frequencies is 9.31 MHz. As demonstrated in [12], more accurate frequency measurement can be achieved by applying the spline interpolation method or using deep neural network assisted frequency estimation.

In conclusion, we have proposed an improved photonic scanning receiver using photonics-based frequency octupling to enlarge the frequency sweeping range and photonic I/Q mixing to measure the signals in two frequency bands that mirror each other. The system can measure the frequencies in a range that is 16 times as large as the electrical sweep source. The system uses up and down chirp frequency sweeping to avoid precise synchronization between the electrical LO and the ADC. The experimental results can verify the feasibility of the proposed system, which is expected to find applications in electronic warfare and communication systems.

**Funding.** National Natural Science Foundation of China (61871214); Natural Science Foundation of Jiangsu Province (BK20180066); Jiangsu Provincial Program for High-level Talents in Six Areas (DZXX-005).

**Disclosures.** The authors declare no conflicts of interest.

## REFERENCES

1. P. W. East, IET Radar Sonar Navigat. **6**, 112 (2012).
2. X. Zou, B. Lu, W. Pan, L. Yan, A. Stöhr, and J. Yao, Laser Photon. Rev. **10**, 711 (2016).
3. H. Chi, X. Zou, and J. Yao, IEEE Photon. Technol. Lett. **20**, 1249 (2008).
4. P. Ghelfi, F. Scotti, D. Nori, and A. Bogoni, IEEE J. Sel. Top. Quantum Electron. **25**, 8900209 (2019).
5. W. Zou, X. Long, X. Li, G. Xin, and J. Chen, Opt. Lett. **44**, 2045 (2019).
6. T. A. Nguyen, E. H. Chan, and R. A. Minasian, Opt. Lett. **39**, 2419 (2014).
7. L. V. Nguyen, IEEE Photon. Technol. Lett. **21**, 642 (2009).
8. X. Zou, W. Li, W. Pan, L. Yan, and J. Yao, IEEE Trans. Microw. Theory Tech. **61**, 3470 (2013).
9. J. Shi, F. Zhang, D. Ben, and S. Pan, IEEE Trans. Microw. Theory Tech. **67**, 544 (2018).
10. J. Shi, F. Zhang, X. Ye, Y. Yang, D. Ben, and S. Pan, Opt. Lett. **44**, 1948 (2019).
11. J. Shi, F. Zhang, D. Ben, and S. Pan, J. Lightwave Technol. **38**, 2171 (2020).
12. Y. Zhou, F. Zhang, J. Shi, and S. Pan, Opt. Lett. **45**, 3038 (2020).
13. J. Ma, J. Yu, C. Yu, X. Xin, X. Sang, and Q. Zhang, Opt. Laser Technol. **42**, 264 (2010).
14. X. Ye, F. Zhang, Y. Yang, and S. Pan, Photon. Res. **7**, 265 (2019).